Eur. Phys. J. E **20**, 449–457 (2006)
DOI 10.1140/epje/i2006-10035-y

THE EUROPEAN PHYSICAL JOURNAL E

Self-assembled pattern formation of block copolymers on the surface of the sphere using self-consistent field theory

J.F. Li, J. Fan, H.D. Zhang, F. Qiu, P. Tang, and Y.L. Yang[a]

The Key Laboratory of Molecular Engineering of Polymers, Ministry of Education of China and Department of Macromolecular Science, Fudan University, Shanghai 200433, PRC

Received 9 March 2006 and Received in final form 5 July 2006 /
Published online: 5 September 2006 –

Abstract. The spherical surface is spatially discretized with triangular lattices to numerically calculate the Laplace-Beltrami operator contained in the self-consistent field theory (SCFT) equations using a finite volume method. Based on this method we have developed a spherical alternating-direction implicit (ADI) scheme for the first time to help extend real-space implementation of SCFT in 2D flat space to the surface of the sphere. By using this method, we simulate the equilibrium microphase separation morphology of block copolymers including AB diblocks, ABC linear triblocks and ABC star triblock copolymers occurred on the spherical surface. In general, two classes of microphase separation morphologies such as striped patterns for compositionally symmetric block copolymers and spotted patterns for asymmetric compositions have been found. In contrast to microphase separation morphology in 2D flat space, the geometrical characteristics of a sphere has a large influence on the self-assembled morphology. For striped patterns, several of spiral-form and ring-form patterns are found by changing the ratio of the radius of a sphere to the averaging width of the stripes. The specific pattern such as the striped and spotted pattern with intrinsic dislocations or defects stems from formed periodic patterns due to microphase separation of block copolymers arranged on the curved surface.

PACS. 83.80.Uv Block copolymers – 36.20.-r Macromolecules and polymer molecules – 68.08.De Structure: measurements and simulations

1 Introduction

Recently phase separation in complex topological space has attracted intensive research interest both experimentally and theoretically due to potential applications in many cellular processes in biology as well as in the design and function of self-assembled morphologies for nanotechnology. For instance, ordered phase-separated domains have been observed at an unprecedented molecular length scale in the ligand shell of nanoparticles [1]. Single and double-helic geometries have been found during the microphase separation of block copolymers confined in cylindrical nano-channels [2]. Recently unique phase separation structures of block copolymers on the spherical nanoparticles have been observed [3].

To date, much theoretical work has been carried out to deal with the influence of the curved space and confinement on the phase separation. Wu *et al.* [2] simulated the microphase separation confined in cylindrical nanochannels based on SCFT and obtained wonderful results in good agreement with experiments. The morphology of symmetric block copolymers in a cylindrical core [4] and asymmetric block copolymers confined in a thin film [5] has been investigated by Fraaijk and Sevink, using the dynamic density functional theory (DDFT). It is found that confinement can induce various intermediate structures in thin copolymer films which are unstable in the bulk phases [5]. These results have been confirmed by the AFM study [6] to some extent. Another elegant method based on Turing Model was used to simulate the periodical patterns on the surface of a sphere [7]. However, as regards the phase separation on the curved surface, due to the mathematical and numerical challenges involved, most of theoretical investigations have been limited and analytical results are derived only for some special classes of surfaces with translation or rotation symmetry [8,9].

In our recently published paper [10], the microphase separation morphology of block copolymers on the spherical surface was obtained by solving Cahn-Hilliard kinetic equation. Unfortunately, this method is phenomenological, which does not consider the detail of the chain topology. SCFT is known to be an appropriate and accurate

[a] e-mail: yuliangyang@fudan.edu.cn

theory to be used for self-assembled morphologies of block copolymers. In fact, SCFT has been successful in predicting the morphologies of diblock copolymers as well as those of linear and star triblock copolymers in the flat space due to the advent of real-space implementation of SCFT [11–14]. However, to our knowledge, most of the present SCFT calculations [11–14] were performed in the flat space because it is difficult to design an alternating-direction implicit (ADI) [15] algorithm in curved space, which is the key to numerically solve the diffusion equation in the SCFT calculation. In this paper, our primary objective is to extend the ADI scheme in the flat space to the surface of a sphere. To achieve this, the sphere is first spatially discretized with triangular lattices so that the Laplace-Beltrami operator contained in the diffusion equation can be readily obtained by using a finite volume method. Based on this discretization method, the whole spherical surface is wrapped up with six closed paths and the spherical ADI scheme can be obtained similar to that in the flat space. Actually, this implementation of the ADI method on the surface of a sphere can also be used to deal with many other physical problems such as heat exchange, quantum mechanics and so on.

In this article, we will firstly present the SCFT theory of block copolymers on the surface of the sphere and focus on the derivation of the spherical ADI scheme on the triangular lattices of the sphere in Section 2. Subsequently, self-assembled morphologies of AB diblock, ABC linear and star triblock copolymers on the spherical surface are investigated with real-space implementation of SCFT on the spherical surface. A series of beautiful striped patterns and spotted patterns of block copolymers will be shown in Section 3. Finally, we have the conclusions in Section 4.

2 Theoretical model and formation

In this section, we present the real-space implementation of SCFT in spherical surface for diblock copolymers and focus on extensions of the alternating-direction implicit (ADI) algorithm to solve the non-linear parabolic diffusion equation in 2D flat space to the surface of a sphere.

Consider a 2D model with n AB linear diblock copolymers each of polymerization N, with compositions (average volume fraction) f_A and $f_B = 1-f_A$ on the surface of a sphere with radius R. The interacting chains on the sphere are reduced to that of independent chains subject to an external (mean) field created by the other chains according to the self-consistent mean-field theory. The fundamental quantity to be calculated in SCFT is the polymer segment probability distribution function $q(\mathbf{r}, s)$, representing the probability of finding a segment s at position $\mathbf{r}$. It satisfies a modified diffusion equation.

For the diffusion equation on the curved surface, the Laplacian in flat space ∇^2 should be replaced with the covariant Laplacian, Δ_{LB}, also known as the Laplace-Beltrami operator [16]. In the spherical surface, thereby, the diffusion equation is given [17,18] by

$$\frac{\partial q(\mathbf{r}, s)}{\partial s} = \frac{a^2}{6}\Delta_{LB} q(\mathbf{r}, s) - [\gamma_A(s)\omega_A(\mathbf{r}) + \gamma_B(s)\omega_B(\mathbf{r})]q(\mathbf{r}, s)\,, \quad (1)$$

where a is the Kuhn length of the polymer segment, $\omega_K(\mathbf{r})$ is the self-consistent field representing the interaction exerted on the species K, and $\gamma_K(s)$ is 1 if s belongs to blocks K and 0 otherwise. The initial condition is $q(\mathbf{r}, 0) = 1$. Because the two ends of diblock chains are distinct, a second end segment probability distribution function $q^+(\mathbf{r}, s)$ is needed. With these descriptions, the free-energy functional of the system can readily be obtained. According to the mean-field approximation, minimizing the free energy with respect to density and pressure leads to the SCFT equation group, which describes the morphology of microphase-separated block copolymers. For more details of SCFT equations of block copolymers, we refer the readers to references [17–19]. In principle, the SCFT equations for a curved surface are exactly the same as those in flat space except that the Laplacian on a curved surface should be replaced with the Laplace-Beltrami operator. Matsen and Schick first numerically solve the SCFT equations with the spectral method [19]. However, this method requires priorly assumed mesophase symmetry and thus the discovery of complex structures is limited. The recent advent of the combinatorial screening algorithm proposed by Drolet and Fredrickson [11,12] has been successfully used to directly solve the SCFT equations. This procedure is iterated until the relative free-energy change at each iteration step is reduced to 10^{-6}. Therefore, the only difference between the real-space implementation of SCFT equations on a spherical surface and that in the flat space is that the ADI technique for solving the diffusion equation for q on a spherical surface is specific and different from the usual one in the flat space. Moreover, it is noted that to avoid the real-space method becoming trapped in a metastable state, random noise is added to the fields to disturb the state formed in the iteration. However, a stable pattern does not depend on the initial self-consistent field. Actually, it is very easy to check out whether any two patterns on the sphere due to the translational degree of freedom are the same morphology with naked eyes, because we can draw the morphologies by using, for instance, 3D drawing software where the sphere can be rotated freely.

Obviously, in the real-space algorithm the computational cost and crucial point to numerical implementation is to solve the diffusion equation and we shall briefly review how to solve the non-linear parabolic diffusion equation in 2D flat space by using the ADI algorithm. In order to implement the Crank-Nicolson algorithm in 2D, which is second-order accurate in both time and space, and unconditionally stable, the ADI scheme [15] in 2D is employed which is an efficient and accurate way to solve the partial parabolic equation. In ADI, the basic idea is to divide each time step (which here denotes the chain contour length Δs) into two steps of size $\Delta s/2$; in each substep, a different dimension is treated implicitly. For example, in 2D flat space an ordinary implicit scheme

for the diffusion equation, $[q(\mathbf{r}, s+\Delta s) - q(\mathbf{r}, s)]/\Delta s = (\frac{a^2}{6}L_x + \frac{a^2}{6}L_y - \omega)[q(\mathbf{r}, s+\Delta s) + q(\mathbf{r}, s)]/2$, can be split into two alternating directions with respect to the orthogonal coordinates x and y:

$$\begin{aligned}
&\left(1 - \frac{a^2\Delta s}{12}L_x + \frac{\Delta s}{4}\omega\right) q\left(\mathbf{r}, s+\frac{\Delta s}{2}\right) = \\
&\qquad \left(1 + \frac{a^2\Delta s}{12}L_y - \frac{\Delta s}{4}\omega\right) q(\mathbf{r}, s)\,, \\
&\left(1 - \frac{a^2\Delta s}{12}L_y + \frac{\Delta s}{4}\omega\right) q(\mathbf{r}, s+\Delta s) = \\
&\qquad \left(1 + \frac{a^2\Delta s}{12}L_x - \frac{\Delta s}{4}\omega\right) q\left(\mathbf{r}, s+\frac{\Delta s}{2}\right)\,,
\end{aligned} \tag{2}$$

where $q(\mathbf{r}, s+\Delta s/2)$ is only an intermedium quantity, *i.e.*, at substep $s+\Delta s/2$ other than the distribution of the chain with chain contour label $s+\Delta s/2$. L_x and L_y denote the discrete form of $\partial^2/\partial x^2$ and $\partial^2/\partial y^2$, respectively. That is to say in 2D orthogonal coordinate, $\nabla^2 = L_x + L_y = \partial^2/\partial x^2 + \partial^2/\partial y^2$. ω is the shorthand of $\gamma_A(s)\omega_A(\mathbf{r}) + \gamma_B(s)\omega_B(\mathbf{r})$. The advantage of ADI is that each substep requires only the solution of a simple tridiagonal system. With these considerations in mind, we will attempt to design an ADI scheme for a spherical surface to solve the diffusion equation numerically.

First, to carry out numerical simulation, a spherical surface is spatially discretized into 20 big spherical triangles generated by the spherical project of the regular icosahedron (with arc sides belonging to the sections of great circles) [10,20]. The further discretization and higher order triangles are obtained by dividing each big spherical triangle into $(L-1)^2$ small triangles with straight sides. In such triangular lattice, each vertex has six neighbors, except for those 12 singular lattice points that belong to the original spherical icosahedron, which have five neighbors each. Actually, any triangulation of sphere surface must exist in excess of exactly 12 fivefold coordinated vertices according to a classic theorem of Euler [21,22]. With this method a discrete sphere surface with $20(L-1)^2$ small triangles and $10(L-1)^2+2$ triangular lattices can be obtained where L must have the form of $3k+1$, where k is an integer. For example, the first five patterns in Figure 3 have 1620 small triangles and 812 triangular lattices where $L = 10$. We have ensured that all these discretizations are with high enough solution accuracy and the discretization with finer triangular grids does not change the patterns. Furthermore, to avoid potential mathematical and numerical problems related to the poles in spherical coordinates, the spherical surface is discretized into almost uniform triangles by employing successive dyadic refinements of the spherical icosahedron. We note that there is no direct correlation between discretization effects and patterns formed in our simulation.

In this paper, a finite volume algorithm is employed to discretize the Laplace-Beltrami operator in the diffusion equation on spherical surface with triangular lattices. Consider the value of a field, say, $X(\mathbf{r})$ the Laplace-Beltrami operator $\Delta_{LB}X$ on the triangular lattice based on averaging Voronoi cells as shown in Figure 1a at the vertex V_0 can be written as [10,23]

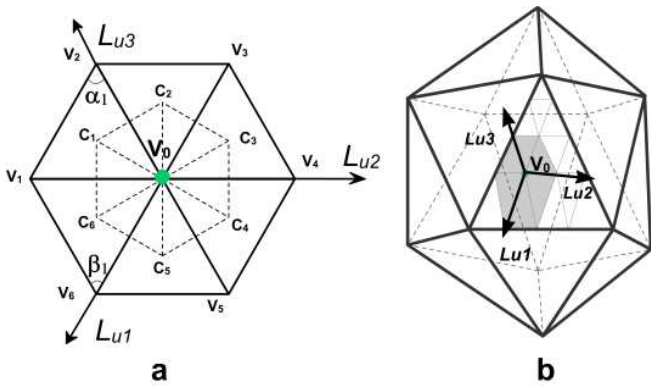

Fig. 1. (a) A vertex with six neighbors and one-ring Voronoi region enclosed by dotted lines for evaluating the Laplace-Beltrami operator Δ_{LB}. Note that $V_1, V_2, \cdots$, and V_6 are not coplanar. (b) The schematic of spherical icosahedron with 20 big triangles used in the spherical ADI scheme.

$$\begin{aligned}
\Delta_{LB}X &= \frac{1}{2A_{Voronoi}}\sum_{i=1}^{6}(\cot\alpha_i + \cot\beta_i)(X_i - X_0) \\
&= \left[R_6X_6 + R_3X_3 - (R_6+R_3)X_0\right] \\
&\quad + \left[R_1X_1 + R_4X_4 - (R_1+R_4)X_0\right] \\
&\quad + \left[R_2X_2 + R_5X_5 - (R_2+R_5)X_0\right],
\end{aligned} \tag{3}$$

where α_i and β_i are two angles opposite to the edges in two triangles sharing the edge V_iV_0 and $R_i \equiv \frac{\cot\alpha_i + \cot\beta_i}{2A_{Voronoi}}$. $A_{Voronoi}$ is the area of the one-ring Voronoi region, which is enclosed by the points $C_1, C_2 \cdots C_6$, as shown in Figure 1a. $A_{Voronoi}$ is obtained:

$$A_{Voronoi} = \frac{1}{8}\sum_{i=1}^{6}(\cot\alpha_i + \cot\beta_i)L_i^2\,, \tag{4}$$

where L_i is the length of the edge V_iV_0. That is to say the discrete Laplace-Beltrami operator at a vertex is the averaging over one-ring neighborhood Voronoi cells. Similar to the discrete form of $\nabla^2X = (\partial^2/\partial x^2 + \partial^2/\partial y^2)X$ in 2D flat space, which can be split into two different directions' summation $(L_x + L_y)X$, the spherical-surface Laplace-Beltrami operator $\Delta_{LB}X$ in equation (3) can also be rewritten as equation (5) by decomposing along three directions (conformational parameter on triangular lattice), where

$$\begin{aligned}
\Delta_{LB} &= L_{u1} + L_{u2} + L_{u3}\,, \\
L_{u1}X &= R_6X_6 + R_3X_3 - (R_6+R_3)X_0\,, \\
L_{u2}X &= R_1X_1 + R_4X_4 - (R_1+R_4)X_0\,, \\
L_{u3}X &= R_2X_2 + R_5X_5 - (R_2+R_5)X_0.
\end{aligned} \tag{5}$$

For 12 vertices of 20 big spherical triangles with only five neighbors, the discrete form of $\Delta_{LB}X$ in equation (3)

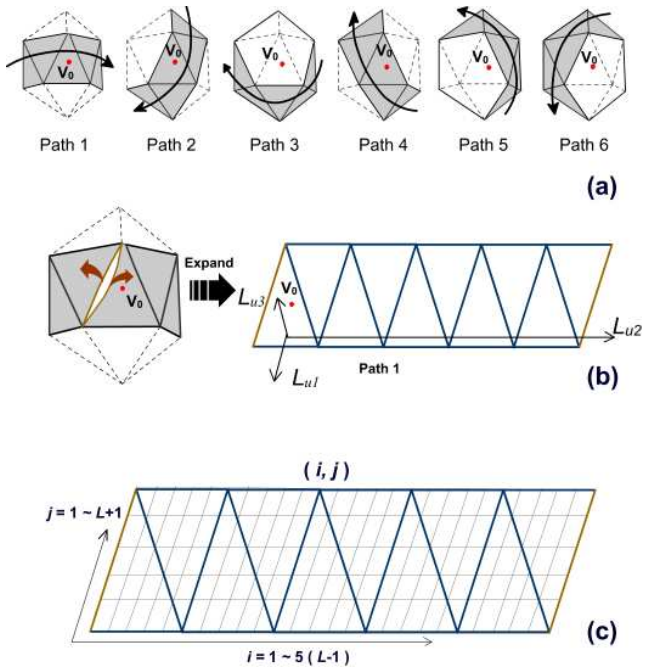

Fig. 2. Schematic illustration of the ADI scheme on the spherical surface. (a) The sphere is wrapped up by six paths. For example, the lattice point V_0 is covered by paths labelled with 1, 2 and 4. (b) Unwrapping of the path 1 which contains ten big triangles. (c) The expansion of each path can be relabelled with (i, j) which is ordinarily used to label the discrete 2D flat space.

can be separated into five directions:

$$\begin{aligned}\Delta_{LB}X &= \frac{1}{2A_{Voronoi}}\sum_{i=1}^{5}(\cot\alpha_i+\cot\beta_i)(X_i-X_0)\\ &= \frac{1}{2}\left[R_5X_5+R_2X_2-(R_5+R_2)X_0\right]\\ &\quad+\frac{1}{2}\left[R_1X_1+R_3X_3-(R_1+R_3)X_0\right]\\ &\quad+\frac{1}{2}\left[R_2X_2+R_4X_4-(R_2+R_4)X_0\right]\\ &\quad+\frac{1}{2}\left[R_3X_3+R_5X_5-(R_3+R_5)X_0\right]\\ &\quad+\frac{1}{2}\left[R_4X_4+R_1X_1-(R_4+R_1)X_0\right]. \qquad (6)\end{aligned}$$

Therefore, the ADI algorithm for the discretization of the Laplacian at a vertex is along three directions L_{u1}, L_{u2}, and L_{u3}, *i.e.*, the triangular mesh itself, similar to that (Eq. (2)) in flat space in form. However, among these three directions only two of them are independent and the remaining one can be linearly expressed by the first two ones. Accordingly, only *two* time steps similar to the case of ADI in 2D flat space are needed to split the original implicit equation in our spherical ADI scheme.

As shown in Figure 2, six paths are used to cover the surface of the sphere and each path includes ten big spherical triangles. It is obvious to find that each big spherical triangle is covered by three paths, and accordingly, the vertex inside each big triangle is covered with three different directions, L_{u1}, L_{u2} and L_{u3}. Note that for the singular vertices with five neighbors, there are five paths going through them while there are four paths for the lattice points on the edges of big triangles and all these lattice points should be treated in a straightforward way. In the following we will show the spherical ADI scheme for the inner lattice points of the big triangles with six neighbors and the extension to the singular lattice point is straightforward. For a vertex $\mathbf{V}_0$ on the discrete sphere (shown in Fig. 2b), the ADI scheme can be treated along three directions labelled with L_{u1}, L_{u2} and L_{u3}. In the L_{u1} direction, the diffusion equation (1) is discretized to obtain the intermedium substep value $q_{u1}(\mathbf{V}_0, s+\Delta s/2)$:

$$\begin{aligned}&\left(1-\frac{a^2\Delta s}{12}L_{u1}+\frac{\Delta s}{6}\omega\right)q_{u1}\left(\mathbf{V}_0,s+\frac{\Delta s}{2}\right)=\\ &\left(1+\frac{a^2\Delta s}{12}L_{u1}+\frac{a^2\Delta s}{6}L_{u2}+\frac{a^2\Delta s}{6}L_{u3}-\frac{5\Delta s}{6}\omega\right)q(\mathbf{V}_0,s).\end{aligned} \qquad (7)$$

Obviously, this equation is very similar to equation (2) in the 2D flat space in form and can be numerically solved because the system is tridiagonal.

The median substep values $q(\mathbf{V}_0, s+\Delta s/2)$ at the lattice point $\mathbf{V}_0$ for the other two directions L_{u2} and L_{u3} are readily obtained in the same form of equation (7). Since these three equations cover all these directions for each lattice point, $q(\mathbf{r}, s+\Delta s)$ on a specific lattice point can only be obtained by averaging the intermedium quantities $q(\mathbf{r}, s+\frac{\Delta s}{2})$ on the paths crossing this lattice point. However, in 2D flat space, because only the direction L_x has been used in the first time step in equation (2), it is possible to construct the second progressive equation with direction L_y:

$$\begin{aligned}q(\mathbf{V}_0,s+\Delta s)=&\left[q_{u1}\left(\mathbf{V}_0,s+\frac{\Delta s}{2}\right)\right.\\ &\left.+q_{u2}\left(\mathbf{V}_0,s+\frac{\Delta s}{2}\right)+q_{u3}\left(\mathbf{V}_0,s+\frac{\Delta s}{2}\right)\right]\Big/3.\end{aligned} \qquad (8)$$

For the lattice points lying on the ridges of big triangles which are crossed four times, there will be four equations on four paths with the same form of equation (7). Two of them are along the same direction but are solved on different paths, and the two intermedium quantities, *i.e.*, the solutions of these two equations will be averaged and put into equation (8). For instance, for a lattice point crossed by paths 1, 2, 3 and 4, paths 1 and 3 are related with the same direction. Accordingly, $q(\mathbf{r}, s+\Delta s)$ can be obtained:

$$\begin{aligned}q(\mathbf{V}_0,s+\Delta s)=&\left[\frac{q_1(\mathbf{V}_0,s+\frac{\Delta s}{2})+q_3(\mathbf{V}_0,s+\frac{\Delta s}{2})}{2}\right.\\ &\left.+q_2\left(\mathbf{V}_0,s+\frac{\Delta s}{2}\right)+q_4\left(\mathbf{V}_0,s+\frac{\Delta s}{2}\right)\right]\Big/3,\end{aligned} \qquad (9)$$

where $q_i(\mathbf{V}_0, s+\frac{\Delta s}{2})$ means the solution on the i-th path other than that on the i-th direction L_{ui}.

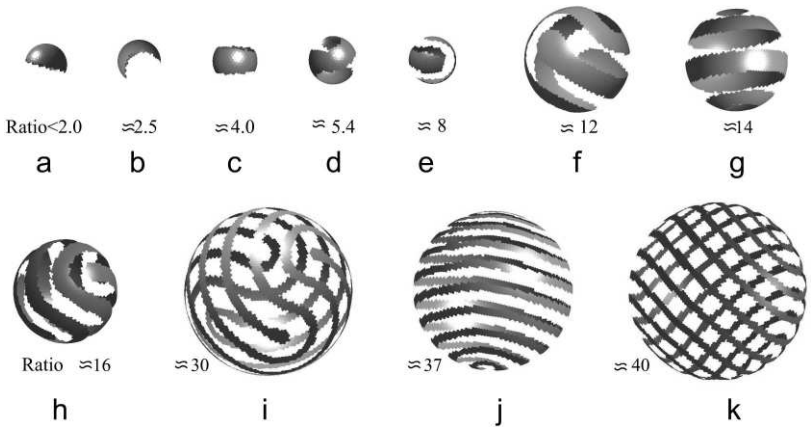

Fig. 3. Typical striped patterns with different ratios of the perimeter of the sphere to average domain size ($2\pi R/D$) for $f_A = 0.5$. For clarity of the arrangement of striped patterns, we only show one component. During the simulations, the discrete lattice number is 812 and $R = 10$ for $2\pi R/D \leq 8$; the lattice number is 4412 and $R = 22$ for $12 \leq 2\pi R/D \leq 16$; the lattice number is 10892 and $R = 34$ for $30 \leq 2\pi R/D \leq 37$; the lattice number is 12962 and $R = 37$ for the last one.

3 Results and discussion

The self-assembled morphology of block copolymers is readily obtained by numerically solving the SCFT equations as we mentioned in Section 2. The extension of SCFT equations and real-space implementation with the ADI scheme on a spherical surface for diblock copolymers to triblock copolymers is straightforward.

3.1 Self-assembled morphology of AB diblock copolymers

Generally, because the phase morphology of AB diblock and ABC triblock copolymers in 2D and 3D flat space as a function of parameters such as copolymer composition, interactions between unlike blocks, etc. has been investigated in detail and the phase diagram has been constructed successfully [13,24], which is very similar to that on spherical surface, the detailed phase diagram in the parameter space on the spherical surface is not presented in this paper, although we have indeed carried out systematic calculations on this. In contrast to microphase separation of AB diblock copolymers in the flat space, the morphology on the spherical surface depends not only on the composition of copolymers and phase segregation strength, *i.e.*, χN, but also on the geometrical characteristics, namely the curvature. In the following will discuss two classes of self-assembled patterns in terms of symmetric and asymmetric composition of block copolymers.

3.1.1 Striped patterns for AB diblocks

For symmetric the composition of block copolymers, *i.e.*, $f_A = f_B = 0.5$, a two-component alternating flat layer structure is formed in the flat space. On the spherical surface, however, various striped patterns dependent on χ, R and sphere radius R are observed. For the sake of simplicity, χN is fixed to be 12. To investigate the relationship between the sphere radius and the domain size, R, N and χN can be put into a single expression, for example, $ratio = 2\pi R/D$, namely the ratio of the perimeter of the sphere to the domain size, which is the unique parameter regulating the morphology of striped patterns alone. Note that D is the average domain size of the microphase related with χ and N and it is roughly estimated by averaging the width of the phase domain.

With increasing the perimeter-domain size ratio, various striped patterns are found as shown in Figure 3. In contrast to the lamellar structure in the flat space, the striped patterns are impossible to be perfect because the sphere cannot be "combed". As pointed out by Varea *et al.* [7] there must be two classes of defects including point defects and line defects. From Figure 3 three classes of striped patterns form including ring-form, spiral-form and cage-form ribbon patterns. As shown in Figures 3a, b, c, e, f and g they can be grouped into ring-form ribbon patterns. Among these patterns Figures 3a, c and g are composed of ordinary ring-form ribbons with point defects at only two opposite sites on the spherical surface, while in Figures 3b, e and f semi-ring ribbons are observed. Patterns in Figures 3d, h, i and j are spiral-form ribbon patterns. In particular, for spiral-ribbon patterns in Figures 3d and j only one spiral-form ribbon crawling on the sphere with two ends (line defects) located at two opposite sites is found. However, though the pattern in Figure 3i is also a single spiral-ribbon pattern, two ends of the ribbon are very close to each other. The double spiral-ribbon pattern in Figure 3h with four defects can be observed very often during our simulations. It is interesting that similar spiral waves were also observed by Gomatam *et al.* [25] in a reaction-diffusion system on a sphere surface. Varea and his coworkers also reported the similar spiral striped patterns on the surface of a sphere in the study of Turing equations [7]. But they have only obtained double spiral-ribbon patterns. Furthermore, cage-form ribbon patterns can be seen when the sphere is large. As shown in Figure 3k, two ribbons are delicately weaved to be a nice cage with front ribbon sections and

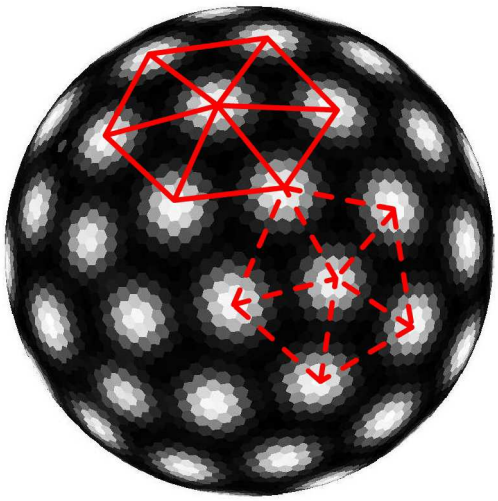

Fig. 4. Spotted pattern of AB diblock copolymers on the surface of sphere with 4412 lattice points. The radius of the sphere is 22, $N = 100$ and $f_A = 0.35$. Color black denotes the B block. The solid lines and dotted lines denote hexagonal and pentagonal spotted patterns, respectively.

back ribbon sections crossing roughly orthogonally. In particular, we note that during innumerable times of simulation symmetric patterns such as the regular ring-form ribbon structure appear only in a very narrow range of perimeter to domain size ratios, namely a certain characteristic ratio so that a number of waves exactly match the sphere size. Finally, it should be noted that some of the simulated patterns such as Figure 3i and Figure 3k are not easy to be predicted without doing calculations. Since the problem of distribution of electrons with repulsive interactions on a sphere [26,27], the so-called Thomson problem, is still not very clear, the distribution of stripes formed by the microphase separation of block copolymers on a sphere may be a more challenging problem. Due to the complexity of these striped patterns and time-consuming computing, the more systematic studies of the morphologies of block copolymers on a spherical surface will be presented in our future works.

3.1.2 Spotted patterns for AB diblocks

For the asymmetric composition of AB diblock copolymers, $f_A = 0.35$, spotted patterns are found as shown in Figure 4. In contrast to the case in 2D flat space where only hexagonal patterns appear, hexagonal lattice structures along with a small number of pentagonal patterns occur due to the geometrical confinement of the spherical surface. Like the dislocations observed in the stripe phase, these defects are intrinsic and cannot be removed by annealing for longer time. Interestingly, recent experimental [21,26] and theoretical results [7,8] demonstrated the similar spotted patterns arrangement on the sphere. Actually, the arrangement of spotted patterns on the sphere is commonly observed in nature, such as atomic and molecular arrangement in crystals [28], virus particles self-assembled on the sphere [29], and so on. The spotted patterns arranged on the sphere will be investigated more carefully and detailedly with the Thomson problem [26, 27] model in our future publications.

3.2 Microphase patterns of ABC triblock copolymers

The extension of SCFT equations and real-space implementation with the ADI scheme on a spherical surface to triblock copolymers is straightforward. Some beautiful striped and spotted patterns of ABC linear and ABC star triblocks have also been calculated by using this new spherical ADI scheme. The radius of the sphere is chosen to be 22 because searching self-assembled patterns on a large-size sphere is not easy and time consuming. Three different colors (namely blue, green and red on-line) represent A, B and C blocks, respectively, in the following figures.

Similar to the case of AB diblock copolymers on the sphere, ABC linear and star triblock copolymers can form striped patterns at some ranges of copolymer composition, as shown in Figure 5 and Figure 6. Ring-form and spiral-form patterns are found depending on the ratio of the perimeter of the sphere to domain size. Furthermore, like the case of triblock copolymers in the flat space the microphase separation on the sphere also depends on the topological structure. For example, for ABC linear triblock copolymers in Figure 5 there are no defects for green on-line ribbons, which means that all the green on-line domains, namely middle blocks, are closed ribbons due to the geometrical character of the sphere. For ABC star copolymers, three blocks within a chain must be jointed at a point and due to this confinement of topology, striped patterns of ABC star triblocks on the sphere can only be observed when Flory-Huggins parameters between blocks are small and one of the blocks is with low composition. As a result, once one of the blocks is with low composition, these striped patterns in Figure 6 are reduced to be the same as those of AB diblock copolymers on the sphere.

Figure 7 and Figure 8 present various spotted patterns for linear and star ABC triblock copolymers. In contrast to the case in 2D flat space where only hexagonal patterns appear, hexagonal lattice structures along with a small number of pentagonal patterns are very common for triblocks on the sphere as shown in Figures 7d and e and Figures 8f and g similar to the case of spotted structure in AB diblock copolymers. At the same time, due to the geometric confinement of the spherical surface the domain on the sphere is often distorted and the size of the domain is distributed inhomogeneously, see in Figure 7f and Figures 8h and i. It is interesting that Fialkowski [30] printed several countries' national-flag patterns onto the microsphere with diameters ranging from 160 μm to 650 μm and it was also found that flags were distorted dramatically.

Finally, it should be noted that when the radius of the sphere is relatively small, the curvature effect on the morphology becomes strong. As shown in Figure 9, when the

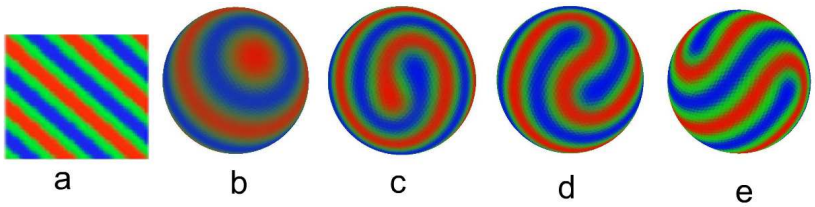

Fig. 5. Comparison of striped patterns in 2D flat space with those on the sphere formed by ABC linear triblock copolymers. (a) Lamellar pattern in 2D flat space [13]. (b) Ring-form ribbon pattern. $N = 200$, $\chi_{AB}N = \chi_{BC}N = 15$, $\chi_{AC}N = 16$, $f_A = f_C = 0.35$ and $f_B = 0.30$. (c) Single spiral-ribbon pattern $N = 100$, $\chi_{AB}N = \chi_{BC}N = \chi_{AC}N = 17$ and $f_A = f_B = f_C = 1/3$. (d) Double spiral-ribbon pattern $N = 100$, $\chi_{AB}N = \chi_{BC}N = \chi_{AC}N = 18$ and $f_A = f_B = f_C = 1/3$. (e) Semi-ring ribbon pattern $N = 100$, $\chi_{AB}N = \chi_{BC}N = \chi_{AC}N = 20$, $f_A = f_B = 0.30$ and $f_C = 0.4$.

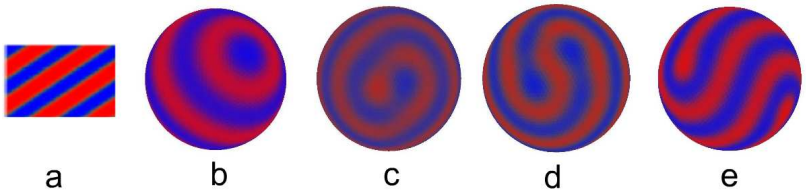

Fig. 6. Comparison of striped patterns in 2D flat space with those on the sphere formed by ABC star triblock copolymers. (a) Lamellar pattern in 2D flat space [14]. (b) Ring-form ribbon pattern $N = 100$, $\chi_{AB}N = \chi_{BC}N = 11$, $\chi_{AC}N = 13$, $f_A = f_C = 0.475$ and $f_B = 0.05$. (c) Single spiral-ribbon pattern $N = 100$, $\chi_{AB}N = \chi_{BC}N = 11$, $\chi_{AC}N = 17$, $f_A = f_C = 0.4$ and $f_B = 0.2$. (d) Double spiral-ribbon pattern $N = 100$, $\chi_{AB}N = \chi_{BC}N = \chi_{AC}N = 18$, $f_A = f_C = 0.4$ and $f_B = 0.2$. (e) Another form of double spiral-ribbon pattern $N = 100$, $\chi_{AB}N = \chi_{BC}N = \chi_{AC}N = 15$, $f_A = f_C = 0.45$ and $f_B = 0.1$.

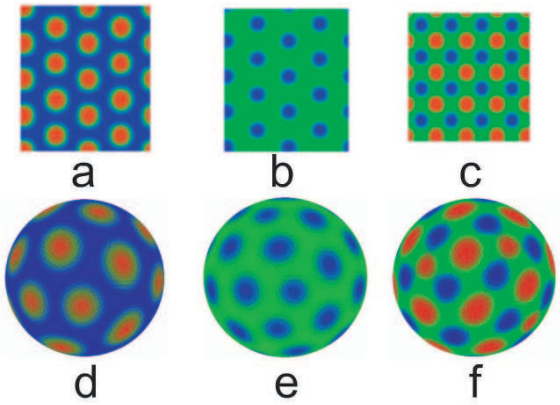

Fig. 7. Comparison of regular spotted patterns in 2D flat space with those on the sphere formed by ABC linear triblock copolymers. Top: spotted patterns in 2D flat space [13]. Bottom: spotted patterns on a spherical surface. (d) $N = 100$, $\chi_{AB}N = \chi_{BC}N = 25$, $\chi_{AC}N = 17$, $f_A = 0.60$, $f_B = 0.20$, $f_C = 0.20$. (e) $N = 100$, $\chi_{AB}N = \chi_{BC}N = 18$, $\chi_{AC}N = 22$, $f_A = 0.30$, $f_B = 0.55$, $f_C = 0.15$. (f) $N = 100$, $\chi_{AB}N = \chi_{BC}N = \chi_{AC}N = 22$, $f_A = 0.25$, $f_B = 0.5$, $f_C = 0.25$.

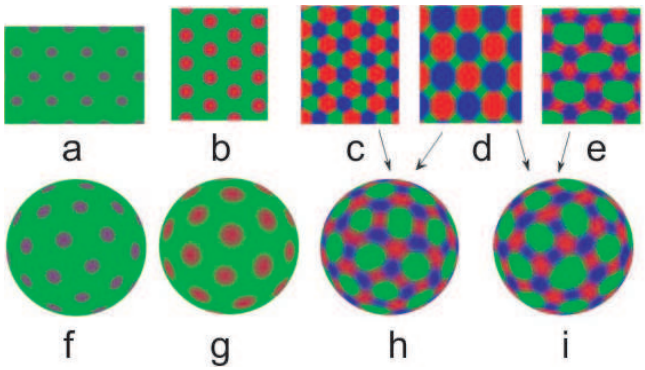

Fig. 8. Comparison of regular spotted patterns in 2D flat space with those on the sphere formed by ABC star triblock copolymers. Top: spotted patterns in 2D flat space [14]. Bottom: spotted patterns on a spherical surface. (f) $N = 100$, $\chi_{AB}N = \chi_{BC}N = \chi_{AC}N = 40$, $f_A = 0.10$, $f_B = 0.80$, $f_C = 0.10$. (g) $N = 100$, $\chi_{AB}N = \chi_{BC}N = \chi_{AC}N = 25$, $f_A = 0.10$, $f_B = 0.70$, $f_C = 0.20$. (h) and (i) have the same average volume fraction and polymerization: $f_A = 0.10$, $f_B = 0.70$, $f_C = 0.20$ and $N = 100$. (h) $\chi_{AB}N = \chi_{BC}N = 25$, $\chi_{AC}N = 20$. (i) $\chi_{AB}N = \chi_{BC}N = 28$, $\chi_{AC}N = 22$.

sphere radius is set to be $R = 10$, for instance, the watermelon pattern for linear ABC triblocks in Figure 9a and perfect three-color cube projection onto spherical surface pattern for star ABC triblocks in Figure 9b are found, which are not observed in the flat space. Figure 9c is the expanded form of the cube projected on the sphere. From this figure it is clearly seen that it is impossible to obtain this pattern in the flat space.

4 Conclusion

We have proposed a spherical alternating-direction implicit (ADI) scheme for the first time to help extend real-space implementation of the self-consistent field theory (SCFT) in 2D flat space to the surface of the sphere. To achieve this objective, the spherical surface is spatially discretized with triangular lattices to numerically calculate the Laplace-Beltrami operator using a finite volume

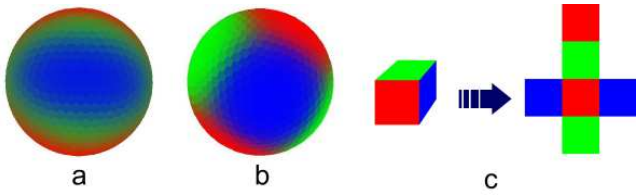

Fig. 9. Special morphologies when the sphere radius is relatively small ($R = 10$). (a) Watermelon pattern formed by ABC linear triblocks. $N = 400$, $f_A = f_B = f_C = 1/3$ and $\chi_{AB}N = \chi_{BC}N = \chi_{AC}N = 20$. (b) Three-color cube projection onto spherical surface pattern formed by ABC star triblocks. $N = 600$, $f_A = f_B = f_C = 1/3$ and $\chi_{AB}N = \chi_{BC}N = \chi_{AC}N = 35$. (c) The expanded form of the cube projected on the sphere.

method. According to icosahedral triangular discretion, the sphere is wra-pped up with six closed paths, each with ten big spherical triangles, and each triangular lattice is covered by three of these paths. In this spherical ADI scheme, therefore the Laplace-Beltrami operator can be treated implicitly along these directions, similar to the ADI in 2D flat space.

With the spherical ADI scheme we perform SCFT calculations for AB diblock copolymers with both symmetric and asymmetric compositions. For the symmetric composition of diblock copolymers, a two-component alternating flat layer structure forms in the flat space. In contrast to the lamellar patterns in 2D flat space, however, the striped patterns on the spherical surface are impossible to be perfect and there must be two classes of defects including point defects and line defects depending on the perimeter of the sphere to the averaging domain size ratio. With increasing ratio of the perimeter of the sphere to the average domain size, ring-form, spiral-form and cage-form ribbon patterns are obtained. For more symmetric patterns, such as the ring-formed structure with fewer dislocations appear at a very narrow range near the characteristic perimeter-domain size ratio. For the asymmetric composition of AB diblock copolymers, spotted patterns can be obtained but with dislocations compared to the case in 2D flat space because of the coupling between the curvature and the commensurability of copolymer period and geometrical period of the spherical surface. For example, a small number of hexagonal lattice structures in 2D flat space change to be pentagon lattice phase. For self-assembled morphologies of ABC linear and star triblock copolymers on the spherical surface, it is found that microphase separation of triblocks also depends on the topological structure just like the case of triblock copolymers in the flat space. However, in contrast to the case in 2D flat space, the periodic patterns must be imperfect, especially the spotted domain on the sphere is often distorted and the size of the domain is distributed inhomogeneously due to the geometric confinement of the spherical surface. Moreover, when decreasing the radius of the sphere to be even smaller, some of the special patterns on the sphere, *e.g.*, watermelon pattern and perfect three-color cube projection onto sphere pattern occur, which are not found in 2D flat space. This discrimination can be interpreted as influences of coupling between the confinement and the big curvature of spherical surface upon the microphase separation of block copolymers.

Furthermore it is also possible to extend this spherical ADI scheme to solve SCFT equations to investigate the microphase separation of block copolymers confined in the spherical shell with thickness or the entire inner space of the sphere. At last as a new numerical algorithm the spherical ADI scheme can also be used to deal with many other physical problems such as heat exchange, quantum mechanics, formation of biological patterns and so on.

We thank financial support from the National Basic Research Program of China (Grant No. 2005CB623800), the "Shuguang" Project of Shanghai Education Development Foundation, the National Special Fund for Excellent PhD Dissertation of China (Grant No. 200124) and for Excellent Research Group of NSF of China. The NSF of China (Grant Nos. 20474012, 20474011, 20374016 and 20104002) is also acknowledged.

References

1. A.M. Jackson, J.W. Myerson, F. Stellacci, Nature Mater. **3**, 330 (2004).
2. Y.Y. Wu, G.S. Cheng, K. Katsov, S.W. Sides, J.F. Wang, J. Tang, G.H. Fredrickson, M. Moskovits, G.D. Stucky, Nature Mater. **3**, 816 (2004).
3. H. Yabu, T. Higuchi, M. Shimomura, Adv. Mater. **17**, 2062 (2005).
4. G.J.A. Sevink, A.V. Zvelindovsky, J.G.E.M. Fraaije, H.P. Huinink, J. Chem. Phys. **115**, 8226 (2001).
5. H.P. Huinink, J.C.M. Brokken-Zijp, M.A. van Dijk, G.J.A. Sevink, J. Chem. Phys. **112**, 2452 (2000).
6. M.A. van Dijk, R. van den Berg, Macromolecules **28**, 6773 (1995).
7. C. Varea, J.L. Aragon, R.A. Barrio, Phys. Rev. E **60**, 4588 (1999).
8. Y. Jiang, T. Lookman, A. Saxena, Phys Rev. E **61**, R57 (2000).
9. Y. Jiang, T. Lookman, A. Saxena, Biophys. J. **78**, 182A (2000).
10. P. Tang, F. Qiu, H.D. Zhang, Y.L. Yang, Phys. Rev. E **72**, 016710 (2005).
11. F. Drolet, G.H. Fredrickson, Phys. Rev. Lett. **83**, 4317 (1999).
12. F. Drolet, G.H. Fredrickson, Macromolecules **34**, 5317 (2001).
13. P. Tang, F. Qiu, H.D. Zhang, Y.L. Yang, Phys. Rev. E **69**, 031803 (2004).
14. P. Tang, F. Qiu, H.D. Zhang, Y.L. Yang, J. Phys. Chem. B **108**, 8434 (2004).
15. W.H. Press, B.P. Flannery, S.A. Teukolsky, W.T. Vetterling, *Numerical Recipes* (Cambridge University Press, Cambridge, England, 1989).
16. D.R. Nelson, T. Piran, S. Weinberg, *Statistical Mechanics of Membranes and Surfaces* (World Scientific, Singapore, 1989).
17. E.J. Helfand, J. Chem. Phys **62**, 999 (1975).
18. S.F. Edwards, Proc. Phys. Soc. London **85**, 613 (1965).
19. M.W. Matsen, M.Schick, Phys. Rev. Lett. **72**, 2660 (1994).

20. J.R. Baumgardner, P.O. Frederickson, SIAM J. Numer. Anal. **22**, (1985) 1107.
21. A.R. Bausch, M.J. Bowick, A. Cacciuto, A.D. Dinsmore, M.F. Hsu, D.R. Nelson, M.G. Nikolaides, A. Travesset, D.A. Weitz, Science **299**, 1716 (2003).
22. T. Kohyama, D.M. Kroll, G. Gompper, Phys. Rev. E **68**, 061905 (2003).
23. M. Meyer *et al.*, *VisMath Proceedings, Berlin, Germany, 2002*, `http://multries.caltech.edu/pubsd/diffGeorOps.pdf`.
24. M.W. Matsen, F.S. Bates, Macromolecules **29**, 1091 (1996).
25. J. Gomatam, F. Amdjadi, Phys. Rev. E **56**, 3913 (1997).
26. M. Bowick, A. Cacciuto, D.R. Nelson, A. Travesset, Phys. Rev. Lett. **89**, 185502 (2002).
27. J.J. Thomson, Philos Mag. **7**, 237 (1904).
28. D.R. Nelson, Nano Lett. **2**, 1125 (2002).
29. T. Stehle, S.J. Gamblin, Y.W. Yan, S.C. Harrison, Structure **4**, 165 (1996).
30. M. Fialkowski, A. Bitner, B.A. Grzykowski, Nature Materials **4**, 93 (2005).